

# Parametric study on the effect of structural and geotechnical properties on the seismic performance of integral bridges

Semih Erhan<sup>1</sup> · Murat Dicleli<sup>2</sup>

Received: 15 October 2015 / Accepted: 15 March 2017 / Published online: 21 March 2017  
© Springer Science+Business Media Dordrecht 2017

**Abstract** In this paper practical techniques are introduced for detailed modeling of soil–pile and soil–abutment interaction effects for integral bridges (IBs). Furthermore, a parametric study is conducted to determine appropriate structural configurations and geotechnical properties to enhance the seismic performance of IBs. For this purpose, numerous nonlinear structural models of a two-span IB including dynamic soil–bridge interaction effects are built. Nonlinear time history analyses (NTHA) of the IB models are then conducted using a set of ground motions with various intensities. In the analyses, the effect of various structural and geotechnical properties such as foundation soil stiffness, backfill compaction level, pile size and orientation, abutment height and thickness are considered. The results of NTHA are then used to assess the effects of these properties on the seismic performance of IBs in terms of member forces and deformations. It is found that while the proposed modeling techniques for IBs are easy to implement in commercially available structural analysis programs, they are also computationally efficient. However, the proposed structural model may not be used to study the soil deformations along the length of the embankment. For the IB and modeling approach under consideration, the bridge seismic response is found to be insensitive to the length of the embankment and damping of the embankment soil. Furthermore, IBs built with shorter and thinner abutments as well as large steel H-piles oriented to bend about their strong axis exhibit better seismic performance.

**Keywords** Seismic · Integral bridge · Parametric study · Abutment · Backfill · Piles · Soil

---

✉ Murat Dicleli  
mdicleli@metu.edu.tr

<sup>1</sup> Department of Civil Engineering, University of Bahrain, Isa Town, Bahrain

<sup>2</sup> Department of Engineering Sciences, Middle East Technical University, Ankara, Turkey

## 1 Introduction

Integral bridges (IBs) are jointless bridges where the deck is built monolithically with the abutments. Arch bridges, rigid-frame bridges, culverts and modern IBs having a single row of steel H-piles at the abutments to provide the required lateral flexibility under thermal effects can be classified as IBs. IBs were first considered after observing the successful performance of older bridges with inoperative expansion joints under seismic and service loads (Palemo et al. 2011; Wotherspoon et al. 2011). Since then, IBs are usually considered as a prime alternative to conventional jointed bridges. IBs have recently become very popular in North America and Europe as they provide many economical and functional advantages (Bhowmick 2003; Spyrakos and Loannidis 2003; Ahn et al. 2011; Zordan et al. 2011; Scott et al. 2013; Franchin and Pinto 2014; Briseghella and Zordan 2015). More than 10,000 IBs are in service today in the US (Maruri and Petro 2005; Fayyadh et al. 2011). Consequently, in the last decade, many research studies have been conducted on IBs. Most of these research studies are concentrated on the performance of IBs under thermal loads (Faraji et al. 2001; Kalayci et al. 2012), live load distribution among the components of IBs (Dicleli and Erhan 2011), soil–structure interaction effects in IBs (Petursson and Kerokoski 2013) as well as state of art and practice of IB design (Arockiasamy et al. 2004). However, in spite of these research studies, standard analysis and design methods for IBs have not been fully established yet. Bridge engineers use the provisions for regular jointed bridges in bridge design specifications such as AASHTO LRFD (2010) and some general design concepts, which are commonly accepted for IBs in practice, to design these bridges. This also includes the seismic design of IBs.

Modern IBs are known to have performed well in recent earthquakes due to the increased redundancy, larger damping resulting from cyclic soil–pile–structure interaction, smaller displacements and elimination of unseating potential (Itani and Sedarat 2000). The monolithic construction of IBs also provides better transfer of seismic loads to the backfill and pile foundations. However, similar to their performance under thermal effects, the seismic performance of IBs may depend on abutment height and thickness, pile size and orientation, backfill compaction level as well as stiffness of the foundation soil. A comprehensive seismic research study on IBs has not been conducted yet to provide clear suggestions for the configuration and geometric detailing of IB structural components as well as appropriate backfill and foundation soil properties to enhance their seismic performance. Accordingly, this research study is aimed at investigating the effect of various structural and geotechnical properties and parameters on the seismic performance of IBs and proposing practical modelling tools for their seismic analysis. The results of this parametric study are then used to propose appropriate structural configurations and geotechnical properties for IBs to enhance their seismic performance. Bridge design engineers may then use the outcome of this research study to configure IBs in their design so as to enhance their seismic performance.

## 2 Research scope and outline

The scope of this research study is limited to straight slab-on-prestressed-concrete girder IBs with no skew. The abutments at both ends of the bridge are assumed to be identical and supported by end bearing steel H-piles. Typical granular backfill used in bridge construction is assumed behind the abutments. The abutments are assumed to be in full contact

with the backfill. Furthermore, cohesionless soil (sand) resting on bedrock is assumed for the simulation of free-field effects of the foundation soil as well as dynamic soil–pile interaction.

To study the seismic performance of IBs as a function of various structural and geotechnical parameters, a two span benchmark IB is considered. Numerous three-dimensional (3-D) nonlinear structural models of the IB including dynamic soil–bridge interaction effects are built using the commercial structural software (SS) SAP2000 (2010) by varying several structural and geotechnical parameters. In the nonlinear structural models, the foundation soil is modelled as a shear column (soil-column) with dashpots to simulate free-field effects and dynamic  $p$ – $y$  curves and dashpots connected between the piles and the soil-column are used to simulate local soil–pile interaction effects and radiation damping. The nonlinear dynamic abutment–backfill interaction is also modelled using an extension of shear column for foundation soil together with nonlinear springs and dashpots. The nonlinear behaviour of the pier columns and steel H-piles at the abutments are modelled using appropriate hysteresis rules available in the SS. The nonlinear time history analyses (NTHA) of the structural models are then conducted using seven ground motions recorded on rock and scaled to various peak ground accelerations. In the analyses, the effect of various structural and geotechnical properties on the seismic performance of IBs is investigated by varying structural and geotechnical properties such as abutment height and thickness, pile size and orientation, foundation soil stiffness and backfill compaction level. However, although the effect of dead load is included in the analyses, the effect of parameters such as those related to the various service load types (e.g. uniform temperature variation, temperature gradient etc.) are not considered in this study. The seismic performance of IBs are then studied in terms of the maximum backfill pressure, maximum relative displacements and rotations of the abutments and piers, maximum absolute displacements of the deck as well as moment, axial forces, absolute displacements and plastic end rotations of the steel H-piles at the abutments. The analyses results are then used to provide suggestions for the structural and geotechnical properties of IBs so as to improve their seismic performance.

### 3 Properties of the benchmark integral bridge and parameters considered in this study

A two span benchmark IB is considered to investigate the effect of various geotechnical and structural properties on the seismic performance of IBs. The benchmark bridge was designed by one of the authors and it was built in 2000. The bridge is on Highway 400 underpass at Major Mackenzie drive in Ontario, Canada. The bridge was originally designed in compliance with Ontario Highway Bridge Design Code. The design of the bridge was modified according to the spectrum and design peak ground acceleration (0.35  $g$ ) considered in this study in compliance with AASHTO (2010). Details of the design are very extensive and can be found in Erhan (2011). The elevation view of the benchmark IB is illustrated in Fig. 1. The total length of the bridge is 82 m and its width is 16 m. The bridge has two spans with lengths of 41 m each and a slab-on-prestressed concrete girder deck. The bridge deck is composed of seven AASHTO type VI girders spaced at 2.4 m and supporting a 225 mm thick reinforced concrete slab. A 75 mm thick asphalt pavement is provided on the deck surface (Fig. 1b). The bridge pier is composed of three 1400 mm diameter circular reinforced concrete columns supporting a cap beam

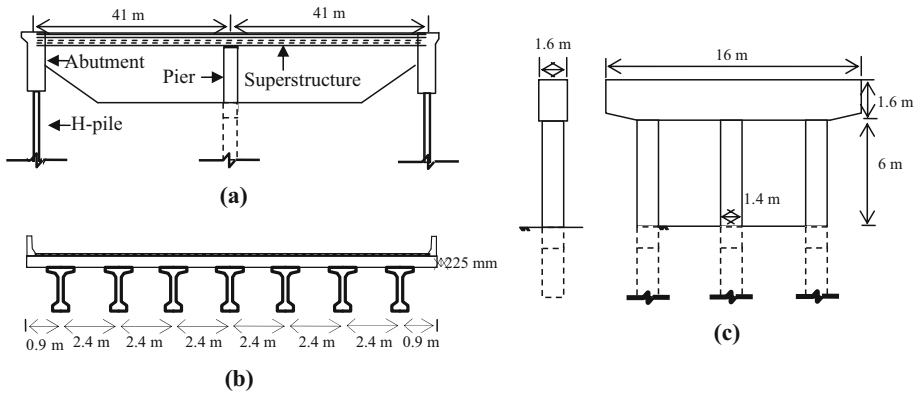


**Fig. 1** a Elevation, b deck cross section and c pier cross section of the IB

(Fig. 1c). The abutments of the benchmark IB are 4 m tall, 1.5 m thick and supported by  $12 \times 15$  m long end-bearing steel HP 310  $\times$  174 piles oriented to bend about their strong axes. The strength of the concrete used for the prestressed concrete girders is 50 MPa while the strength of the slab, abutment and pier concrete is 30 MPa. The granular compacted backfill behind the abutments is assumed to have a unit weight of  $20 \text{ kN/m}^3$ . The foundation soil surrounding the piles is assumed to be medium sand.

For the parametric study, the stiffness of the foundation soil (sand) is anticipated to affect the seismic performance of IBs. Thus, four different soil stiffness values (loose, medium, medium-dense and dense sands) are considered in the analyses. Furthermore, to investigate the effect of abutment geometry on the seismic performance of IBs, three different abutment heights (3, 4 and 5 m) and abutment thicknesses (1, 1.5 and 2 m) are considered in the analyses. To assess the effect of pile size on the seismic performance, the analyses are repeated using pile sizes of HP 310  $\times$  174 and HP 250  $\times$  85. Moreover, the steel H-piles are also assumed to be oriented to bend about their strong and weak axes to study the effect of pile orientation on the seismic performance of IBs. In addition, both compacted (unit weight  $20 \text{ kN/m}^3$ ) and uncompactd (unit weight  $18 \text{ kN/m}^3$ ) backfill behind the abutments are considered in the analyses to study the effect of backfill compaction level on the seismic performance of IBs. The parameters considered in this study are tabulated in Table 1.

**Table 1** Parameters considered in the analyses

Parameters	Description
Pile size	HP 310 $\times$ 174 (LP), HP 250 $\times$ 85 (SP)
Pile orientation	Strong axis (SA) and weak axis (WA) bending
Abutment thickness (m)	1, 1.5, 2
Abutment height (m)	3, 4, 5
Soil stiffness	Loose, medium, medium-dense and dense sand
Backfill compaction level	Compacted and uncompactd backfill

## 4 Selected ground motions

For the NTHA of the IBs considered in this study, seven earthquake ground motions whose response spectra are compatible with the AASHTO (2010) spectrum for soil type I (Rock) are selected from the PEER (Pacific Earthquake Engineering Research) strong motion database of the University of California, Berkeley. The main reason for considering soil type I (Rock) in the analyses is that the ground motions are applied at the base of the piles at the bedrock level and the free-field effect of the foundation soil above the bedrock is considered separately in the structural model using an equivalent soil-column. The design peak ground acceleration at the site is assumed to be 0.35 g and the design spectrum is built based on this acceleration. The AASHTO design spectrum and spectra of the ground motions considered in this study are scaled to 0.35 g peak ground acceleration and presented in Fig. 2. The ground motions considered in this study are selected such that the average of their spectra resembles the AASHTO spectrum within the range of fundamental periods of vibrations of the benchmark IB considered in this study (0.32–1.26 s.) (Figure 2). The second criteria in the selection of the ground motions is to have ground motions with a wide range of  $A_p/V_p$  ratio ( $A_p/V_p = 6.05\text{--}30$ ) covering earthquakes with a wide range of frequency content while nearly matching the AASHTO design spectrum within the range of vibration periods of interest. In this way, the effects of a wide range of earthquakes on the seismic response of IBs are represented. Details of the selected ground motions are given in Table 2. The ground motions are scaled to have peak ground accelerations of 0.2, 0.35, 0.5 and 0.8 g to study the effect of various structural and geotechnical properties on the seismic performance of IBs, as a function of the earthquake intensity. Amplitude scaling is used to scale the ground motions to a given peak ground acceleration level. Accordingly, the acceleration time histories of the ground motions are first divided by their peak ground acceleration, and then multiplied by specific peak ground acceleration values used in the parametric analyses.

## 5 Nonlinear structural modeling of integral bridges

To investigate the effect of various structural and geotechnical properties on the seismic performance of IBs, 3-D nonlinear structural models of the IBs considered in this study are built using the aforementioned SS. A 3-D model is especially necessary to study the response of IBs in the transverse direction including the transverse direction responses of the wing-walls, backfill, piers and piles (to simulate the frame action of the piers and piles in the transverse direction), which are not possible to simulate accurately in a 2-D model.

**Fig. 2** The comparison of the AASHTO design spectrum and acceleration spectra of the selected earthquakes

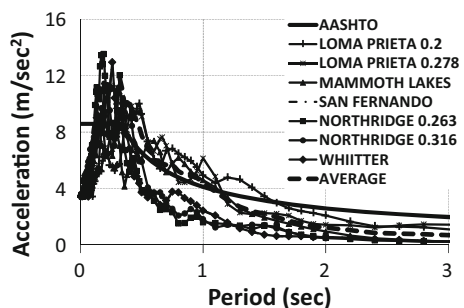


**Table 2** Properties of the selected ground motions

Earthquake	Station/component	Magnitude	Distance (km)	$A_p$ (g)	$V_p$ (cm/s)	$A_p/V_p$ (1/s)
Loma Prieta, 1989	58222SF-Presidio	6.9	83.1	0.20	32.4	6.05
Loma Prieta, 1989	1601 Palo Alto-SLAC Lab	6.9	36.3	0.28	29.3	9.2
Mammoth Lakes, 1980	54214 Long Valley Dam (Upr L Abut)	6.0	20.0	0.41	33.9	11.8
San Fernando, 1971	266 Pasadena-Old Seismo Lab	6.6	19.1	0.20	10.9	18.2
Northridge, 1994	24592 LA, City Terrace, 090	6.7	37.0	0.26	12.8	20.2
Northridge, 1994	24592 LA, City Terrace, 180	6.7	37.0	0.32	14.1	23.4
Whitter, 1987	108 Carbon Canyon Dam (L Abut)	6.0	26.8	0.20	6.5	30

Even though, a 3-D model is used, the ground motions are applied one at a time in each direction to avoid complicated coupled response so as to facilitate the understanding the effect of each structural and geotechnical parameter on the seismic response of the bridge. Various modelling features of the SS such as compression only springs, gap elements, Pivot, Takeda as well as Plastic Wen nonlinear hysteretic link elements facilitated the simulation of complex behavioral types such as nonlinear behavior of backfill and foundation soil and inelastic hysteretic behavior of structural members such as reinforced concrete piers and steel piles. In the following subsections, the details of these 3-D nonlinear structural models are presented.

### 5.1 Modeling of superstructure

The bridge superstructure is modelled using 3-D beam elements as shown in Fig. 3a. Full composite action between the slab and the girders is assumed. The superstructure is divided into a number of segments and its translational (23.36 tons/m) and rotational mass is lumped at each nodal point connecting the segments. At the abutment and pier locations, the bridge deck is modeled as a transverse rigid bar of length equal to the center-to-center distance between the two exterior girders supporting the deck slab. The transverse rigid bar is used to simulate the interaction between the axial deformation of the columns and torsional rotation of the bridge deck as well as the interaction between the in-plane rotations of the deck and relative displacements of the bearings.

### 5.2 Modeling of bearings

The bearings considered in this study are regular low damping rubber bearings. It is a known fact that in this type of bearings loading and unloading paths nearly overlap; that is, their behavior is linear elastic (Warn and Ryan 2012). Accordingly, the lateral stiffness of the bearing is calculated by the following equation:

$$K_b = \frac{G_R A_b}{h_b} \quad (1)$$

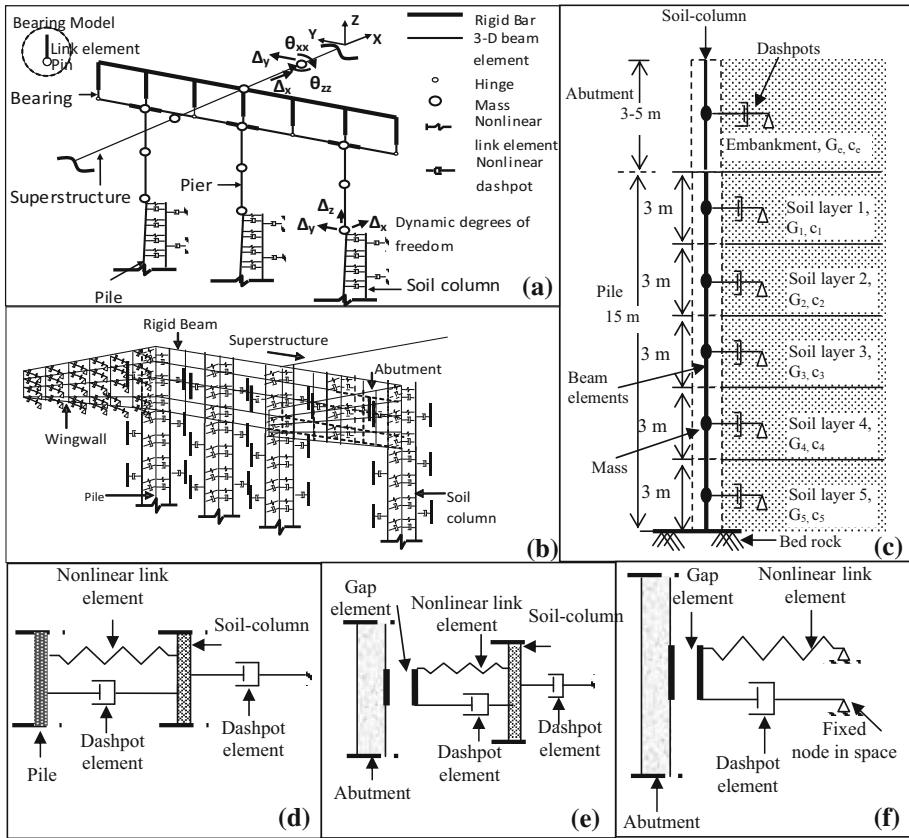


**Fig. 3** **a** Structural modeling details at the pier and bearings, **b** structural modeling details at the abutments, **c** soil-column modeling details, **d** soil-pile interaction modeling, **e** abutment-backfill interaction modeling with embankment, **f** abutment-backfill interaction modeling without embankment

In the above equation,  $G_R$  is the shear modulus of rubber material,  $A_b$  is the bonded plan area of the rubber bearings and  $h_b$  is the thickness of the rubber bearing (or height of the rubber).

The calculated lateral stiffness of the bearing is increased by a factor of 1.35 to obtain an effective shear stiffness ( $K_b = 1.35x K_{bmin}$ ) that considers the effect of aging and low temperature conditions throughout the service life of the bridge. This calculated lateral stiffness of the bearing is implemented in the SS by link elements with linear properties.

### 5.3 Modeling of pier, reinforced concrete piles, abutments and steel H-piles

The reinforced concrete cap beam, columns and piles underneath the piers are modeled as 3-D beam elements (Fig. 3a). The program X-TRACT (2009) is used to obtain the moment curvature relationships of the pier columns of the IB considered in this study. The moment curvature relationships are then used in a nonlinear hinge (Link) element in the SS to define the envelope of the hysteresis loops simulated by the Takeda model (Takeda et al. 1970). Typical hysteretic behavior of the pier column is illustrated in Fig. 4a. It is noteworthy that a capacity design approach is used to prevent plastic hinging and hence damage to the

piles. Thus, plastic hinging is assumed only in the pier columns. The abutments are modeled using a grid of frame elements as shown in Fig. 3b. The program X-TRACT (2009) is also used to obtain the moment curvature relationship of the abutments of the bridges considered in this study. These diagrams are used as envelopes of hysteresis loops to simulate the nonlinear behavior of the abutments in the structural models using the Takeda model (Takeda et al. 1970). However, the NTHA of the IBs revealed that plastic moment hinging does not occur in the abutments. This is mainly due to the fact that the steel H-piles and the backfill yield before any yielding occurs in the abutment. In the transverse direction, wingwalls are similarly modeled using a grid of frame elements as shown in Fig. 3b. The steel H-piles are also modeled using frame elements. The current state of design practice does not use capacity design approach to prevent plastic hinging in the steel H-piles at the abutments under seismic excitations. This is mainly due to the much larger size and associated larger flexural capacity of the abutments compared to that of the piles. Therefore, the cyclic behavior of steel H-piles is modeled using an elasto-plastic hysteretic behavior using Plastic-Wen link element (Dicleli 2007). Typical hysteretic behavior of the steel H-piles is illustrated in Fig. 4b.

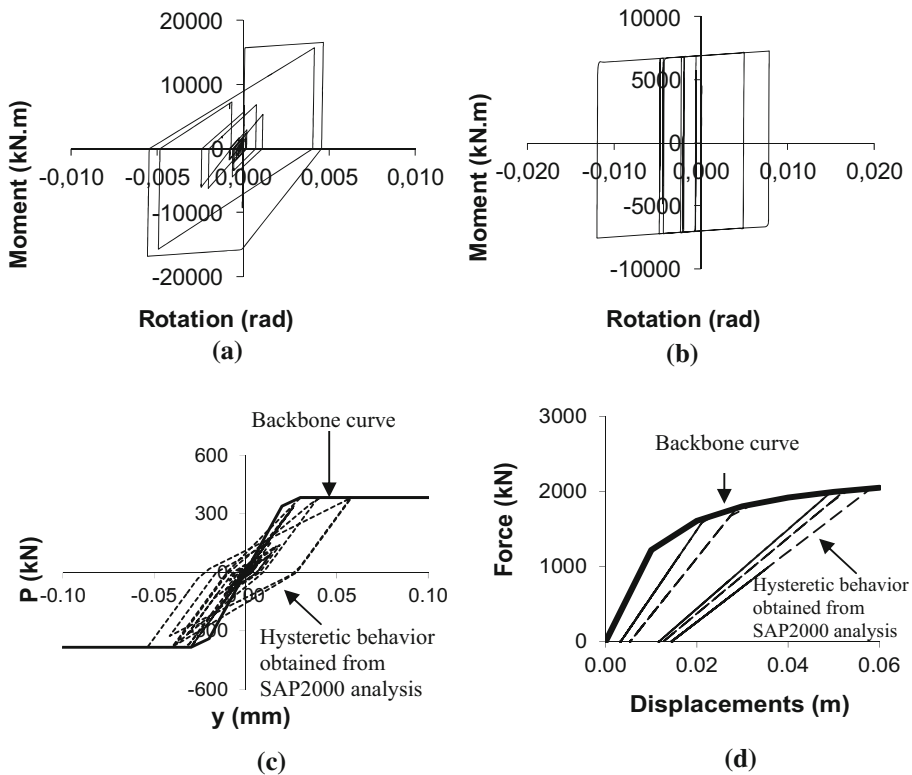


**Fig. 4** **a** Typical pier column moment-rotation hysteresis loop, **b** typical steel H-pile moment rotation hysteresis loop, **c** sample hysteresis loop simulating soil-pile interaction from SAP2000 analyses, **d** sample hysteresis loop simulating abutment-backfill interaction from SAP2000 analyses (San Fernando Earthquake  $A_p = 0.8$  g)



## 5.4 Modelling of soil–bridge interaction

It is a known fact that soil–pile and abutment–embankment interaction simulation is an important structural modeling aspect of seismic response prediction of IBs. There are several ways of simulating the soil–pile and abutment–embankment interaction in the structural model of IBs. For instance, one way is to build a complex 3-D finite element model of the foundation and embankment soil using a specialized software capable of modeling both nonlinear structural and continuum soil elements as well as surface contact interactions and conducting nonlinear time history analysis for soil materials (Zhang and Makris 2002; Kotsoglou and Pantazopoulou 2007, 2009, 2010). For such finite element models, if a coarse mesh is selected, the level of accuracy will be lost (Shamsabadi 2007). However, when a refined mesh is used, the model becomes very tedious to build and computationally require extensive run times. Therefore, such complex models are generally not used in engineering practice (Shamsabadi 2007) and are not employed in this research study as the main focus of the research study is the structural response rather than the response of the foundation soil and embankment. Accordingly, the soil–bridge interaction is simulated in the structural model by using a soil–column model.

The soil–column modeling approach employed in this study consists of replacing the continuum soil elements with a soil–column having spring–dashpot components that are attached to the frame model of the bridge structure and its pile foundation. The local nonlinear force–displacement behavior of springs and viscous damping coefficients of the dashpots at the soil–pile and abutment–backfill contact interfaces are obtained from research studies involving models generated via calibration with experimental results. The properties of the soil–column to simulate the free-field behavior of the foundation soil (degraded shear modulus and equivalent damping ratios) for a given ground motion scaled to a specific peak ground acceleration are obtained by modeling separately the foundation soil and approach embankments with specialized software for soil response analysis.

The research studies of Franchin et al. (2007) and Franchin and Pinto (2014) revealed that the soil–column model is capable of providing reasonably good predictions of both maximum and residual bending moments of structural members and their cumulative displacements. Furthermore, Zhang and Makris (2002) have compared the dynamic properties of a 3-D model of a long embankment with that of a 1D tapered soil–column and found that soil column approximation captures most of the longitudinal and transverse response of the approach embankment in comparison to the 3-D models. On the other hand, the main disadvantage of the soil–column modeling approach for the embankment is that it fails to estimate the deformations along the length of the embankment and associated soil damping. However, as the main focus of this study is the structural response of the IB, the deformations along the length of the embankment were not of interest. Nevertheless, sensitivity analyses are conducted to determine the effect of the embankment itself (a model with and without embankment) as well as its length (mass) and damping on the structural response and the results are reported in Sect. 5.4.3.1.

The soil–bridge interaction model used in this study could be classified into three forms. The first one is the local abutment–backfill interaction where the interaction between the backfill and the laterally moving abutment under seismic effects is considered locally. The second one is the local soil–pile interaction where the interaction between the pile and soil under seismic effects is simulated locally by so called  $p$ – $y$  curves. The third one is the free-field motion of the foundation soil and the embankment (backfill) with respect to the

bridge, which is considered by using a soil–column in the structural model. Details of the modeling procedures for these three soil–bridge interaction forms are given below.

#### 5.4.1 Modeling of local abutment–backfill interaction

The local abutment–backfill (and in the transverse direction wingwall–backfill) interaction behavior under cyclic loads is simulated using the hysteresis model proposed by Cole and Rollins (2006) that takes into consideration possible formation of a gap behind the abutment at each loading cycle (as the abutment pushes towards the backfill and pulls back under seismic effects). In this hysteresis model, first the hyperbolic load ( $P$ )–deflection ( $Y$ ) envelope curve for the abutment–backfill system must be defined. The following hyperbolic  $p$ – $y$  relationship purposed by Duncan and Mokwa (2001) is used for this purpose:

$$P = \frac{y}{\frac{1}{K_{max}} + R_f \frac{y}{P_{ult}}} \quad (2)$$

where  $P$  is the passive resistance of backfill,  $P_{ult}$  is the ultimate passive resistance,  $y$  is the backfill deformation,  $K_{max}$  is the initial slope of the load–deformation curve and  $R_f$  is the failure ratio assumed as 0.85 (Duncan and Chang 1970).

In the SS, the pivot model (Dowell et al. 1998) is used to simulate the hysteretic behavior of the backfill behind the abutment by assigning appropriate values to the hysteresis model parameters. The pivot hysteresis model (Dowell et al. 1998) requires the force–deformation envelope (for the backfill defined by Eq. 2) as well as two additional parameters for capturing the pinching and stiffness degradation effects. In the hysteresis model, “ $\alpha$ ” refers to the stiffness degradation parameter and “ $\beta$ ” corresponds to pinching parameter. However, in the full scale tests performed by Cole and Rollins (2006) on several abutment–backfill systems, no pinching behavior is observed. Accordingly, pinching effect is excluded from the pivot model by setting  $\beta = 1$ . The parameter  $\alpha$  in the pivot model is calculated from the intersections of the two consecutive unloading lines  $K_{r1}$  and  $K_{r2}$  and corresponding permanent displacements  $\Delta_{s1}$  and  $\Delta_{s2}$  in the backfill hysteresis model proposed by Cole and Rollins (2006) as shown in Fig. 5b to simulate the force–displacement behavior of the backfill. Accordingly, in the structural model, the hysteretic behavior of the abutment backfill system is simulated by using nonlinear link elements with pivot hysteresis model connected between the nodes along the length of the abutment and the soil–column for the case where the embankment is included in the structural model (with embankment) (Fig. 3e). However, for the case where the embankment is not included in the structural model (without embankment), while one end of the nonlinear link element is connected to the abutment, the other end is attached to a node fixed in space (Fig. 3f). A typical abutment–backfill hysteresis loop obtained from the analyses is presented in Fig. 4d.

The radiation damping effects (as the abutment impacts the backfill) for the abutment–backfill system is simulated in the structural model using dashpots (Fig. 3e, f). The radiation damping coefficient for these dashpots is obtained from the following equation proposed by Jain and Scott (1989).

$$c = \sqrt{\frac{2}{1 - \nu}} G \rho \quad (3)$$

where  $G$ ,  $\rho$  and  $\nu$  are the dynamic shear modulus, mass density and Poisson’s ratio of the backfill respectively. In the analyses  $G$ ,  $\rho$  and  $\nu$  are taken as 6000 kN/m<sup>2</sup>, 2.05 ton/m<sup>3</sup> and

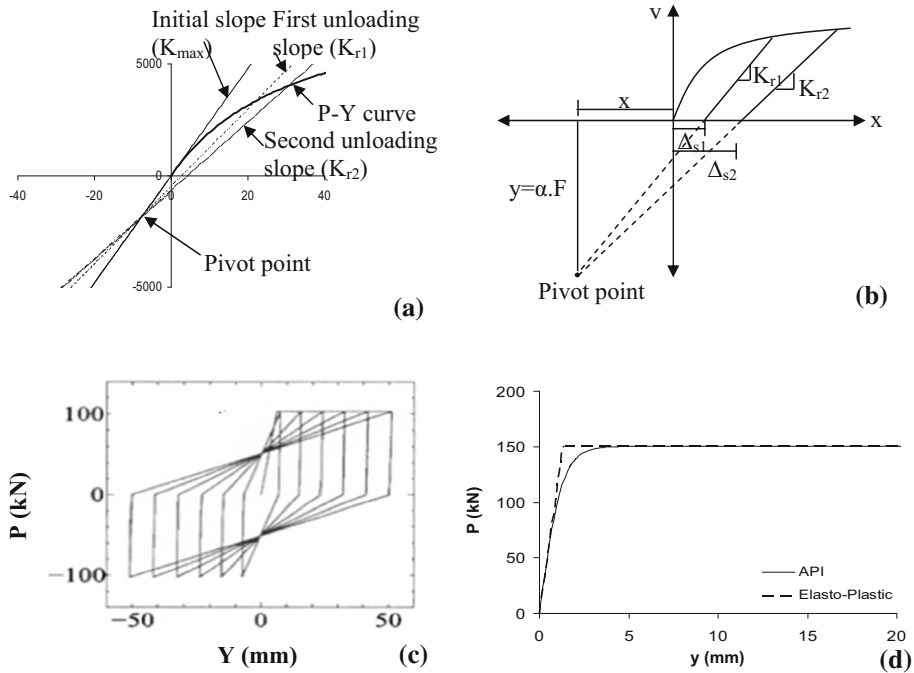


**Fig. 5** **a** Hysteretic abutment-backfill interaction diagram, **b** pivot parameter of  $\alpha$ , **c** Hysteretic soil–pile interaction diagram proposed by Shirato et al. (2006), **d** Elasto-plastic envelope  $p$ - $y$  curves for soil–pile interaction

0.3 respectively for compacted backfill. For the uncompacted version of the backfill  $G$ ,  $\rho$  and  $\nu$  are taken as  $5000 \text{ kN/m}^2$ ,  $1.84 \text{ ton/m}^3$  and 0.3 respectively. During seismic excitation, there is a compression-only interaction between the abutment and backfill. Accordingly, gap elements with a zero gap length connected in series with the nonlinear links and dashpots are incorporated in the structural model to simulate this behavior (Fig. 3e, f).

5.4.2 Modeling of local soil–pile interaction

The local soil–pile interaction behavior under cyclic loads is simulated using the hysteresis model proposed by Shirato et al. (2006). In this hysteresis model, first a monotonic load–deflection envelope curve must be defined. The lateral soil resistance–deflection ( $p$ – $y$ ) relationship for sand available in API (2001) is used to define this envelope curve at any specific depth,  $H$  as follows:

$$P = A_f P_u \tanh \left[ \frac{kH}{A_f P_u} y \right] \tag{4}$$

where  $A_f$  is a factor to account for cyclic or static loading condition and assumed as 0.9 for cyclic loading (API 2001),  $P_u$  is the ultimate lateral bearing capacity of the foundation soil at depth  $H$  (kN/m) and  $k$  is the initial subgrade reaction modulus ( $\text{kN/m}^3$ ) given in the API design code (2001) as a function of the angle of internal friction ( $\phi$ ). The properties of the soils used in the analyses are given in Table 3.

**Table 3** The properties of soil types considered in this study

AASHTO soil—sand type	k (kN/m <sup>3</sup> )	$\phi$ (deg)	$\gamma$ (kN/m <sup>3</sup> )	N	G <sub>max</sub> (kPa)	v <sub>s</sub> (m/s)
I—Dense	61,000	38	20	40	224,000	330
II—Medium-dense	40,650	35	19	27	163,400	290
III—Medium	21,680	32	18	18	118,000	250
IV—Loose	2170	29	16	7	55,000	150

In the hysteresis model proposed by Shirato et al. (2006), the envelopes of the p–y curves of the foundation soil are assumed as elasto-plastic (Fig. 5c). The p–y curves obtained from the API (2001) recommendation are also nearly elasto-plastic and hence, suited well for the model proposed by Shirato et al. (2006) as shown in Fig. 5d. The hysteretic rules of the Takeda’s hysteresis model available in the SS are similar to those proposed by Shirato et al. (2006) [unloading curves are parallel to the initial slope of the elasto-plastic p–y curves (Fig. 5c)]. Accordingly, in the structural model, the hysteretic behavior of the soil–pile system is simulated by using nonlinear link elements with Takeda’s hysteresis model connected between the nodes along the length of the pile and the soil-column representing free-field effects (Fig. 3d).

A typical soil–pile hysteresis loop obtained from the analyses is presented in Fig. 4c. To simulate radiation damping as the piles impact the soil under seismic effects, dashpots are placed between the nodal points along the pile and the soil-column representing free-field effects (Fig. 3d). The radiation damping coefficient for these dashpots is obtained from the following equation (Anandarajah et al. 2005).

$$c = A\rho V_s \quad (5)$$

where  $A$  is the tributary area between the nodal points along the pile,  $\rho$  is the mass density of the soil and  $V_s$  is the shear wave velocity.

#### 5.4.3 Modeling of free-field effects (global abutment–backfill and soil-pile interaction) by soil-column model

In bridge design, generally the relative movement of the surrounding soil (free-field motion) during the earthquake is not considered. However, this may result in an incorrect simulation of the overall behavior of the bridge during a potential earthquake especially for soft soil conditions where free-field movements may be considerable (Boulanger et al. 1999). For this purpose, in this study, a soil-column model is used to simulate the relative movement of the surrounding soil around the piles at the pier and abutments as well as the embankments at the abutments (free-field soil) in the structural model.

**5.4.3.1 PROSHAKE model** To obtain the equivalent linear properties (equivalent damping and equivalent degraded shear modulus) of the soil-column model in the SS, first, the foundation soil together with the embankment is modeled using the program PROSHAKE (PS) (2009). The properties of the foundation soil and embankments used in this model are chosen considering the seismic site soil types (Soil Types I–IV) given in AASHTO LRFD Bridge Design Specifications (AASHTO 2010). Each soil type is defined

by two properties; the maximum shear modulus,  $G_{max}$  and the shear wave velocity  $v_s$ , given in Table 3.

In the model, the 15 m deep foundation soil is divided into five three-meter-thick layers. The embankment is also included as a layer on top of the foundation soil with a height equal to the abutment height (varied between 3 and 5 meters depending on the model). Then, time history analyses of the model (free-field soil) are performed using the seven earthquake records used in the analyses. The equivalent degraded shear modulus and equivalent damping ratios at each soil layer and embankment are then obtained from the analyses results for each earthquake and the levels of peak ground accelerations considered in the analyses (7 earthquakes  $\times$  4 peak ground accelerations = 28 cases per soil type). Typical values of equivalent degraded shear modulus and equivalent damping ratios for the embankment and each foundation soil layer obtained from PS analyses are given in Table 4. These parameters are then used to build linear soil-column models integrated with the bridge structural model.

**5.4.3.2 Soil-column model in SAP2000** In the SS, the free field effect of the foundation soil is simulated by introducing three soil columns; one at the pier and one at each abutment. The soil column includes both the free field foundation soil and the embankment. Since the top of the pier piles are at a lower elevation than the abutment piles (5.4 m lower), the connection between the pier piles and the soil column is only along the soil–pile contact length. In the case of the soil column at the abutments however, the connection between the soil column and the piles together with the abutment is along the full height of the soil column.

For the soil-column model in the SS, beam elements (as many discrete beam elements as the number of soil layers and embankment connected in series at nodal points along the height of the soil-column) having a high flexural rigidity but a shear stiffness computed using the equivalent degraded shear modulus obtained from PS analyses is used (Fig. 3c) to simulate the free-field behavior of the foundation soil and the embankment. To determine the stiffness properties of the shear beam elements used in the soil-column model in the SS, first the shear area of the free field soil needs to be determined since the beam stiffness is equal to  $G_{Si} \times A_S$  and  $A_S$  is the shear area of the free field soil. This required a series of analyses as it will be explained later. Using the unit weight, shear area and the height of the soil layer, the mass of each soil layer is calculated and lumped at each node

**Table 4** Typical equivalent degraded shear modulus and damping ratios for each layers of soil-column obtained for San Fernando Earthquake

Depth (m)	Layer description	$A_p = 0.5$ g		$A_p = 0.8$ g	
		Shear modulus (kPa)	Damping ratio	Shear modulus (kPa)	Damping ratio
–2	Embankment	93,568	4.02	85,489	5.23
–5.5	Soil layer 1	75,643	9.03	68,775	10.09
–8.5	Soil layer 2	49,396	11.77	38,094	14.26
–11.5	Soil layer 3	29,740	16.35	19,552	19.46
–14.5	Soil layer 4	20,840	18.97	13,567	21.72
–17.5	Soil layer 5	19,652	19.42	10,637	22.85

along the soil-column. Dashpots are used to simulate the equivalent damping effects in the soil. Next, time history analyses of the soil-columns alone (without the bridge) are performed using the SS and the analyses results are compared with those obtained from PS in Fig. 6a. It is found that the displacement and velocity time histories at the top of the soil-column obtained from the analyses using the SS are generally in good agreement with those obtained from the PS analyses. Thus, the soil-column model is used together with the bridge model to simulate free-field effects.

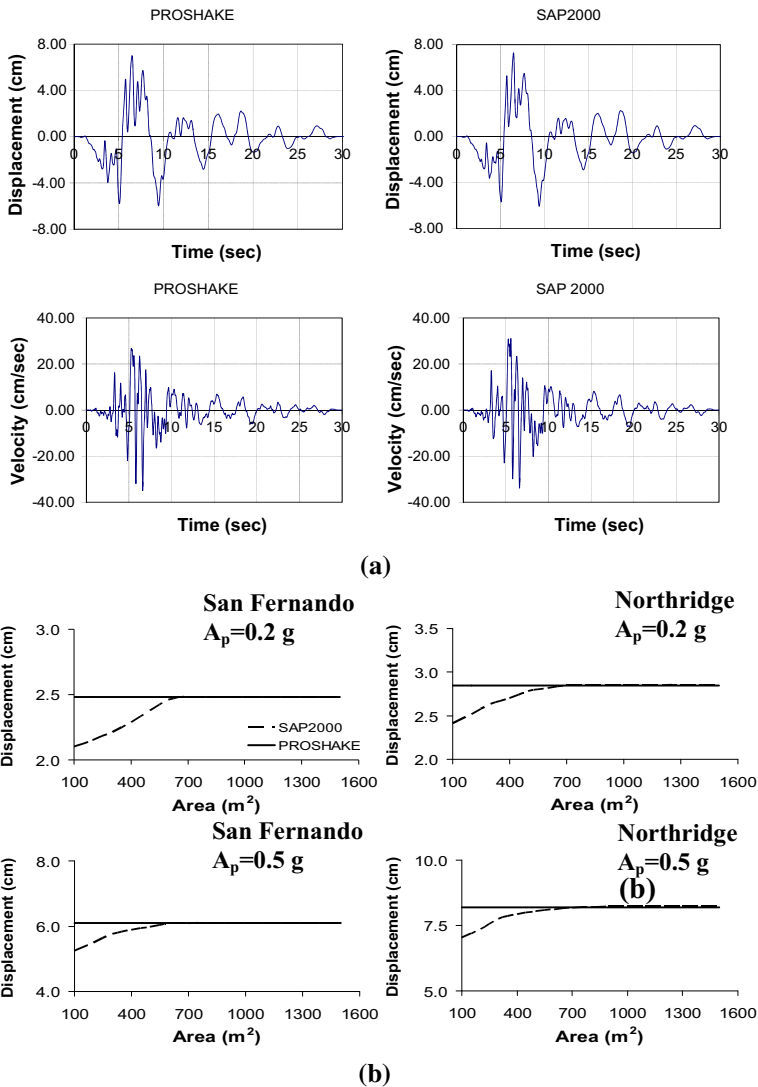


**Fig. 6** **a** The displacement and velocity time histories obtained from PROSHAKE and SAP2000 analyses for San Fernando earthquake for  $A_p = 0.5$ , **b** sensitivity analyses results for shear area of soil-column

**5.4.3.3 Analyses to determine the optimum shear area of the soil for the soil-column model** In the structural model with the bridge and the soil-column, the free-field motion of the foundation soil together with the embankment (e.g. displacements or accelerations of the soil layers simulated by the soil-column) should not be affected by the response of the bridge due to the very large size of the soil field compared to the size of the bridge in actual conditions (the bridge is very small compared to the free-field soil). This could be achieved by selecting a very large shear area for the soil-column in the structural model. However, a too large shear area selected for the soil-column may produce numerical instability during the nonlinear solution procedure as the stiffness of the soil-column will be much larger than those of the structural members of the bridge. Accordingly, in the structural model, the size of the shear area of the soil-column must be selected carefully to prevent such numerical instability during the nonlinear solution procedure. To define the optimum shear area of the soil-columns used in the structural models, sensitivity analyses are conducted. For this purpose, NTHA of various soil-column models having different shear areas together with the bridge model are performed using the SS. Then the maximum top displacements of the soil obtained from PS analyses are compared to those obtained from the analyses using the SS where the soil-column and the bridge are modeled together. As observed from Fig. 6b, the maximum top displacements are found to be almost the same, when the shear area is chosen as larger than or equal to  $650 \text{ m}^2$ . Accordingly, the soil-columns are modeled using frame elements having a shear area of  $650 \text{ m}^2$  together with the bridge model. The area of the embankment in the upper portion of the soil-column is taken as the abutment width times the embankment length (80 m) as proposed by Kotsoglou and Pantazopoulou (2007). However, in the following section, sensitivity analyses are conducted to assess the effect of the embankment itself, its length (mass) and damping on the seismic response of IBs.

**5.4.3.4 Sensitivity analyses for the embankment** In this section, sensitivity analyses are conducted to assess the effect of the embankments on the seismic performance of IBs and to investigate the effect of the assumed embankment size (for different foundation soil depths) and embankment soil damping in the structural model on the seismic response of the IB. For this purpose, first, NLTA of the benchmark bridge are conducted for two different cases where the effect of the embankment is included (with embankment) and excluded (without embankment) from the structural model and the analyses results are presented for various responses.

Figure 7a–f displays the maximum absolute displacement of the deck and relative displacement of the pier bearings with respect to the pier top, pier column drifts (top displacement minus bottom displacement) and end rotations as well as absolute abutment pile displacements and end rotations in the longitudinal direction as a function of the peak ground acceleration for the cases with and without embankments. Although the transverse direction responses are available, they are not reported in the paper due to the fact that the response magnitudes and trends are similar to those in the longitudinal direction. It is observed from the figures that including the embankment in the structural model produces slightly larger deck, bearing, pier, abutment and pile responses. This is mainly due to the larger flexibility at both ends of the IB when the embankment is included in the structural model since the embankment moves together with the soil-column due to ground shaking and the nonlinear backfill link elements representing the local force deformation relationship of the backfill are attached between the abutment and the soil column. However, for the case where the embankment is not included in the structural model (without

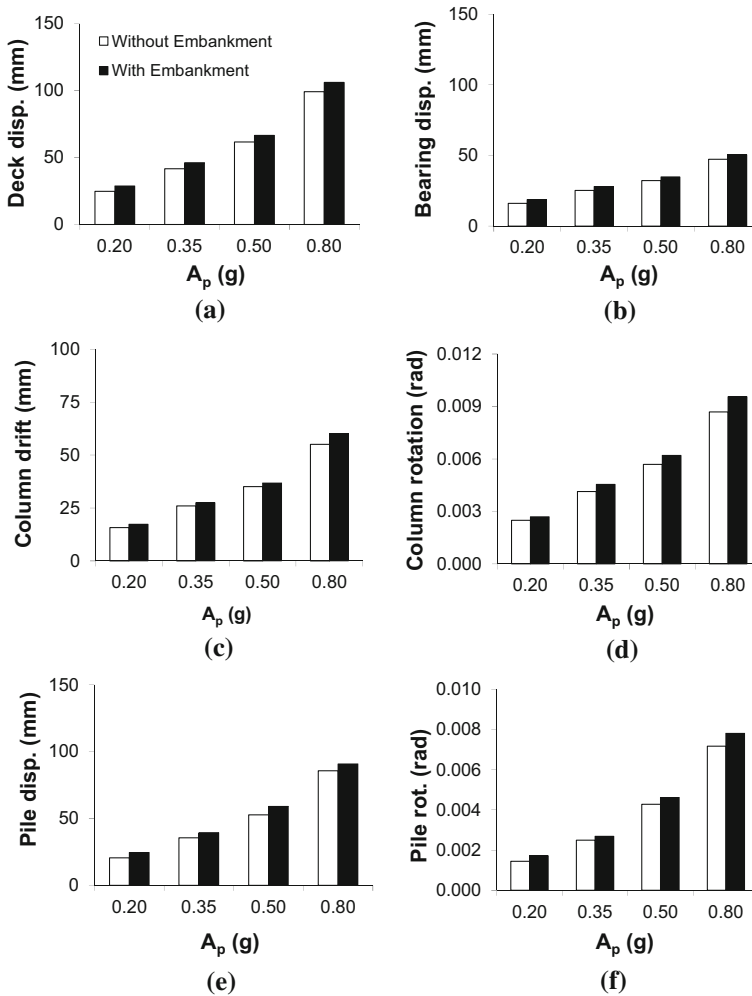


**Fig. 7** **a** Absolute deck displacements, **b** relative bearing displacements, **c** pier column drifts and **d** rotation, **e** absolute steel H-pile displacements and **f** rotations versus peak ground acceleration obtained from the models with and without embankments

embankment) the backfill soil is assumed to be stationary (Backfill soil is not moving with the soil-column). Only the local force–displacement relationship of the stationary backfill is modelled using nonlinear link elements where one end of the link element is connected to the abutment and the other end is attached to a node fixed in space (Fig. 3f). Accordingly, for the case without the embankment, the bridge's longitudinal movement is constrained between the two sets of nonlinear backfill link elements and the bridge can move only as much as the deformation of the nonlinear backfill spring. The maximum difference between the cases with and without embankment occurs at  $A_p = 0.8$  g and is equal to 9% for absolute deck displacement and pier column drift and 7% for absolute abutment pile displacement. However, for the abutment pile axial forces and variation of moment along the piles, the analyses with and without the embankment yielded nearly identical results.



Since including the embankment in the structural model is observed to affect the seismic response of the bridge to a certain extent, all the structural models are built by considering the effect of the embankment.

To investigate the effect of embankment length (mass) and the level of embankment soil damping on the IB model response, sensitivity analyses are conducted. For this purpose, NTHA of the structural models of the benchmark IB having an embankment length of 20, 40, 60, 80 and 100 m are performed. The analyses results are presented in Fig. 8 for various bridge responses. The analyses results revealed that the embankment length has negligible effects on the seismic response of IBs. The main reason for this is that the lower part of the soil-column used to simulate the free-field effect of the foundation soil has a much larger mass and stiffness compared to the upper part of the soil-column for the embankment. Therefore, the dynamic response of the entire soil-column is controlled by the lower part of the soil-column representing the large free-field soil. To test the validity of these findings for a different free field soil depth, the lower five meters part of the foundation soil together with the piles are truncated (now the free field soil depth is only 10 m) and the analyses are repeated for the cases of the IB with large piles oriented in strong axis bending (benchmark bridge) and the IB with small piles oriented in weak axis bending. As the plan area of the free field soil is much larger than that of the embankment, the shallower foundation soil mass and stiffness are still very large leading to comparative results (for different embankment lengths) similar to those observed for the 15 m deep free field soil. Furthermore, to investigate the effect of embankment soil damping on the seismic response of the bridge, analyses are conducted for a damping level 20% smaller and larger than the actual damping level. The analyses results revealed that, for the bridge under consideration, the embankment soil damping effect is less than 4%. Although the analyses results reveal that the effect of embankment mass and damping is not significant, it is important to note that the soil column modeling approach used in this study inherently considers uniform deformations along the embankment length, and hence the observations from the analyses results may be altered when such deformations are considered. However, considering the level of uncertainties in the foundation and embankment soil properties from practical point of view, the soil column modeling approach is considered to be adequate for the purpose of this study. Accordingly, the 80 m embankment length and the level of damping considered in the analyses seem appropriate for the benchmark bridge under consideration.

## 6 Parametric nonlinear time-history analyses results

The 3-D structural models of 16 IBs with various structural and geotechnical properties are built and NTHA of the bridge models are conducted using the seven earthquake ground motions considered in this research study. The IBs considered in this study are fully symmetrical and the analyses are performed separately in the longitudinal and transverse directions. Therefore, possible limitations in the SS in capturing the coupled responses in both orthogonal directions of the bridge in 3-D analyses are not of a concern in this study. The elastic modal periods of IBs with different properties considered in this study are given in Table 5. The NTHA are repeated for each peak ground accelerations considered in this study for each selected earthquake. This led to 460 different analyses cases including the sensitivity analyses for the soil-column modeling. The analysis results of IBs are presented as the average of the results from the seven ground motions for various peak ground

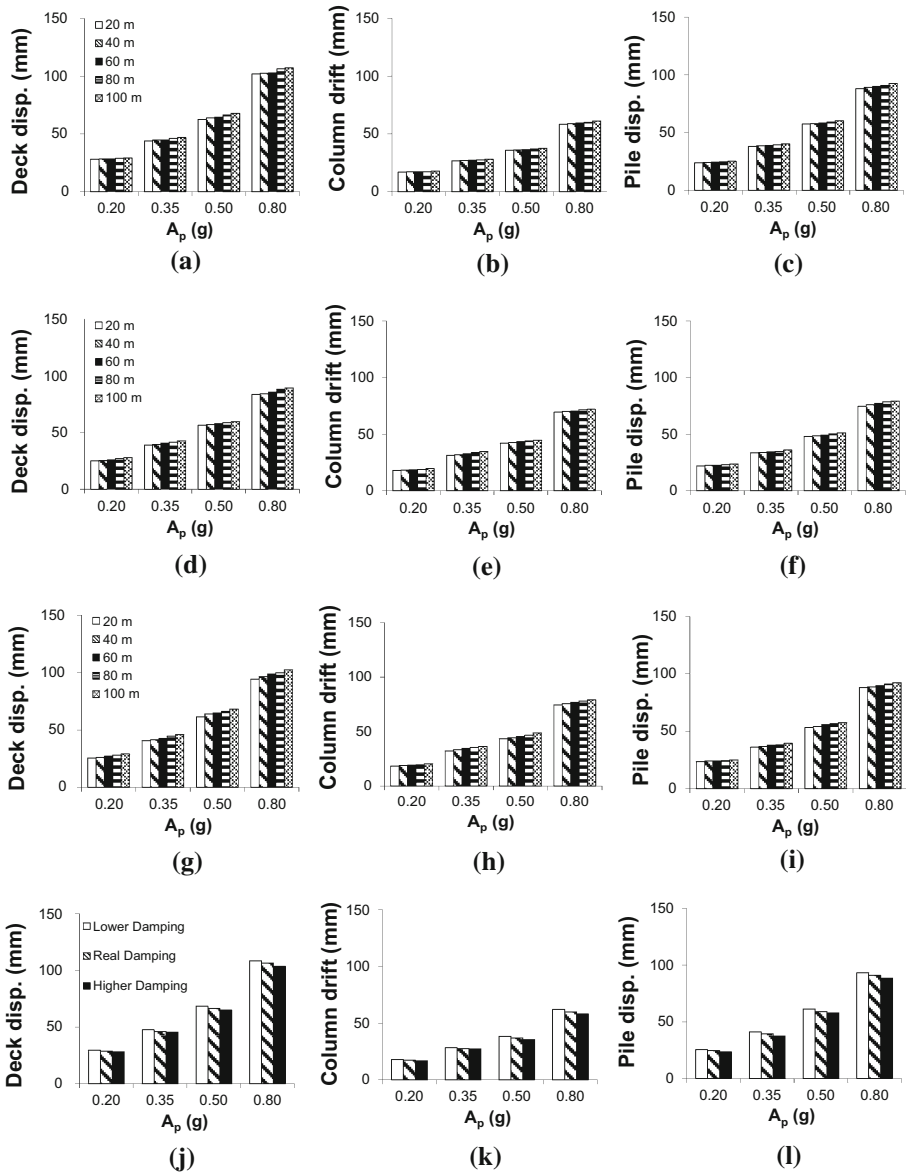


**Fig. 8** Effect of embankment length (20–100 m) on the seismic response of the bridge for a foundation soil depth of 15 m; **a** Absolute deck displacements, **b** pier column drifts and **c** absolute steel H-pile displacements. Effect of embankment length (20–100 m) on the seismic response of the bridge for a foundation soil depth of 10 m. and large piles oriented in strong axis bending; **d** absolute deck displacements, **e** pier column drifts and **f** absolute steel H-pile displacements. Effect of embankment length (20–100 m) on the seismic response of the bridge for a foundation soil depth of 10 m. and for small piles oriented in weak axis bending; **g** Absolute deck displacements, **h** pier column drifts and **i** absolute steel H-pile displacements. Effect of embankment soil damping (20% lower and 20% higher damping) on the seismic response of the bridge: **j** absolute deck displacements, **k** pier column drifts and **l** absolute steel H-pile displacements

**Table 5** Modal periods (s) of the IBs considered in this study

Direction	Soil stiffness			Abutment height (m)					Abutment thickness(m)			Pile size			Pile orientation			Backfill compaction level	
	Dense	M. Dense	Med. Loose	3	4	5	1	1.5	2	2	LP	SP	SA	WA	WA	Comp	Uncomp		
Long.	0.73	0.86	1.79	1.14	1.26 <sup>a</sup>	1.33	1.16	1.26 <sup>a</sup>	1.28	1.26 <sup>a</sup>	1.60	1.26 <sup>a</sup>	1.63	1.26 <sup>a</sup>	1.63	1.26 <sup>a</sup>	1.31		
Trans.	0.25	0.29	0.41	0.26	0.32 <sup>a</sup>	0.38	0.28	0.32 <sup>a</sup>	0.39	0.32 <sup>a</sup>	0.40	0.32 <sup>a</sup>	0.40	0.32 <sup>a</sup>	0.40	0.32 <sup>a</sup>	0.33		

<sup>a</sup> Benchmark bridge values

**Fig. 9** **a** Absolute deck displacements, **b** relative bearing displacements, **c** pier column drifts and **d** rotation, **e** absolute steel H-pile displacements and **f** rotations versus peak ground acceleration for different soil stiffnesses, **g** pile axial forces and **h** typical pile moments for San Fernando Earthquake scaled to  $A_p = 0.8$  g for various foundation soil stiffnesses

accelerations. However, for the pile moments and backfill pressure, the responses are presented only for individual ground motions to facilitate the observation of the actual distribution of the moment along the pile and the backfill pressure along the abutment height.

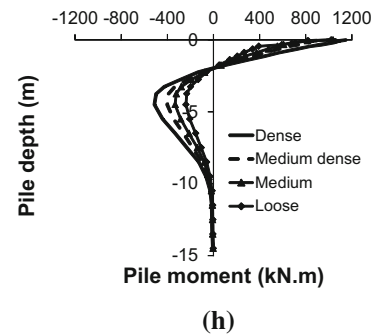
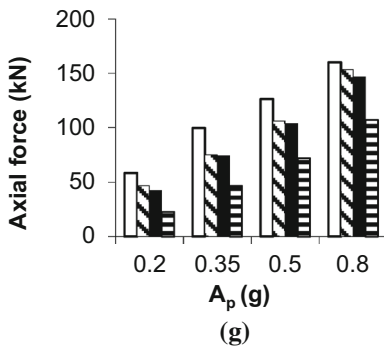
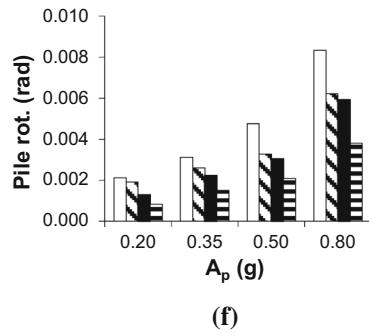
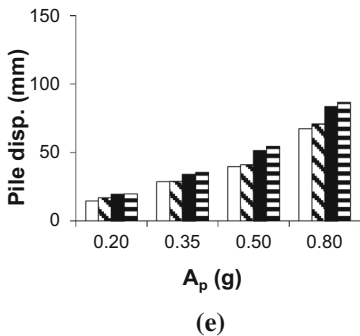
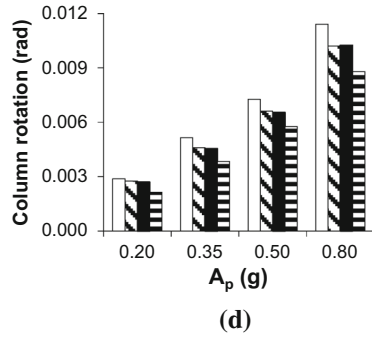
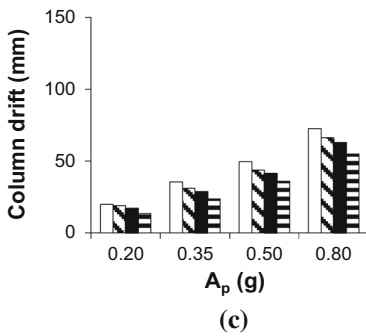
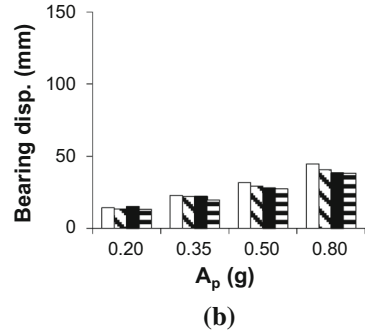
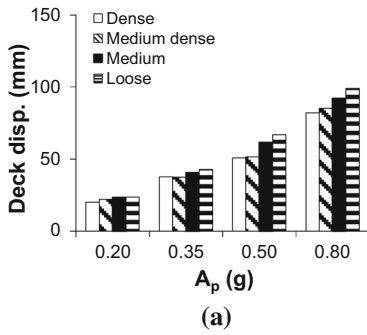
It is noteworthy that the analyses results are only given for the responses that exhibit notable variation as a function of the parameter under consideration. Furthermore, the analyses results reveal that IB responses differ less than 5% for the uncompacted and compacted backfill cases. Accordingly, the effect of backfill compaction level on the seismic performance of IBs is found to be negligible and the results are not presented. In addition, although the transverse direction responses are available, they are not reported in the paper as the response magnitudes and trends are similar to those in the longitudinal direction. In the following subsections, while the deck, bearing, pier and pile responses are reported as a group for each parameter, the responses of the abutments and backfill are reported separately for all the parameters considered in this study. This is mainly done due to the similarity of the trends in the abutment and backfill responses for all the parameters.

### 6.1 Effect of foundation soil stiffness on deck, bearing, pier and pile responses

The effects of the foundation soil stiffness on the deck, bearing, pier and pile responses are displayed in Fig. 9a–h. As observed from the figures, stiffer foundation soils produce smaller absolute deck displacement for IBs. This is mainly due to the larger foundation stiffness in the case of stiff soil conditions producing smaller absolute pile displacements leading to smaller overall bridge or absolute deck displacements.

In the case of bearings and pier columns however, stiffer foundation soil conditions results in larger bearing displacements relative to the pier top (Fig. 9b) and larger column drifts and end rotations (Fig. 9c, d). This could be explained as follows; for stiff soil conditions, the absolute pile displacements are small. This obviously produces higher drift/rotation demands on the pier columns and higher displacement demands on the bearings. Smaller drifts and plastic rotations in the pier columns are indicative of less structural damage and hence better seismic performance. Accordingly, the piers of IBs built on soft soil conditions will experience less damage (better performance) in the case of a potential earthquake. Comparing Fig. 9a with 9b and 9c, the summation of relative bearing displacement and column drift for the same soil type seems to be larger than the absolute deck displacements. This may be possible as the maximum displacements of components do not occur all at the same time and in most cases the absolute displacement of the deck and relative displacements of pier columns/bearings are out of phase. For example, for San Fernando earthquake with  $A_p = 0.5$  g, the maximum positive deck displacement occurred at 6.57 s., but the maximum positive bearing and pier column displacements occurred at 7.21 and 7.17 s respectively.

The analysis results also reveal that larger soil stiffness produce smaller absolute displacements in steel H-piles (please note that this is not a drift but absolute displacement) due to the large rigidity of the pile–soil system (Fig. 9e). For the steel H-pile top rotations however, the opposite is true. That is, larger foundation soil stiffness produce larger plastic rotations in steel H-piles of IBs. In the case of soil conditions, the equivalent pile length,



which is the length of the pile to the point of fixity within the soil, becomes much smaller. This results in much larger plastic rotations since the cord rotations are calculated as the ratio of absolute pile displacement to the equivalent pile length. Accordingly, the steel H-piles of IBs built on soft soils will experience less damage in the case of a potential earthquake.

The maximum axial forces and variation of the typical pile moments along the depth of steel H-piles at the abutments are compared in Fig. 9g, h for various foundation soil stiffnesses. The axial loads given in Fig. 9g are those due to seismic actions only. As observed from the figure, stiffer foundation soils produce larger axial forces in the piles of IBs. This is mainly because of the fact that larger foundation soil stiffness produces larger base moments at the bridge (at the bottom of the substructures). These larger base moments need to be somehow counterbalanced by the axial force couples created in the abutment piles at both ends of the bridge. It is also observed from the figure that the maximum moment occurs at the pile top and in most cases, the pile top moments are the same due to plastic hinge formation. However, larger moments are observed along the depth of the pile in the case of stiffer foundation soil. This is mainly due to the larger stiffness of soil–pile system in the case of stiffer foundation soil creating larger bending effect along the length of the pile as the pile top tries to displace together with the abutment under seismic actions.

## 6.2 Effect of abutment height and thickness on deck, bearing, pier and pile responses

The effects of the abutment height on the deck, bearing, pier and pile responses are displayed in Fig. 10a–f. Although the responses are available for various abutment thicknesses, they are not reported in the paper as the response magnitudes and trends are similar to those obtained for abutment heights.

The analyses results reveal that taller and thicker abutments produce larger absolute deck displacements (Fig. 10a) as well as larger absolute abutment pile displacements and end rotations (Fig. 10c, d). This is mainly due to the larger mass of taller and thicker abutments producing larger inertial forces and associated larger absolute deck displacements as well as larger absolute abutment pile displacements and end rotations. In addition, taller abutments produce larger overall structural flexibility resulting in larger absolute deck displacements. The longer fundamental periods of IBs with taller and thicker abutments (Table 5) also indicate that larger absolute deck displacements as well as larger absolute abutment pile displacements and end rotations are expected for such bridges.

However, the abutment height and thickness are found to have only a negligible effect on the bearing relative displacements as well as pier column drifts and end rotations. This could be explained as follows: For IBs with taller and thicker abutments, the absolute deck displacement is large. However, this higher displacement demand is distributed among the piles, columns and bearings at the piers. Consequently, the relative displacement of the bearings and pier column drifts and rotations are not notable (Please note that the contribution of small differences in the bearing, pier column drifts and the displacement at the top of the piles underneath the piers produce large differences between the absolute deck displacements for various abutment heights and thicknesses but not between the bearings).

The maximum axial forces and variation of the typical pile moments along the depth of steel H-piles at the abutments are compared for various abutment heights in Fig. 10e, f. The figures reveal that taller abutments produce larger axial forces in the piles of IBs especially in the case of large intensity ground motions. Similar results are observed for larger abutment thicknesses. This is mainly because of the fact that larger abutment heights

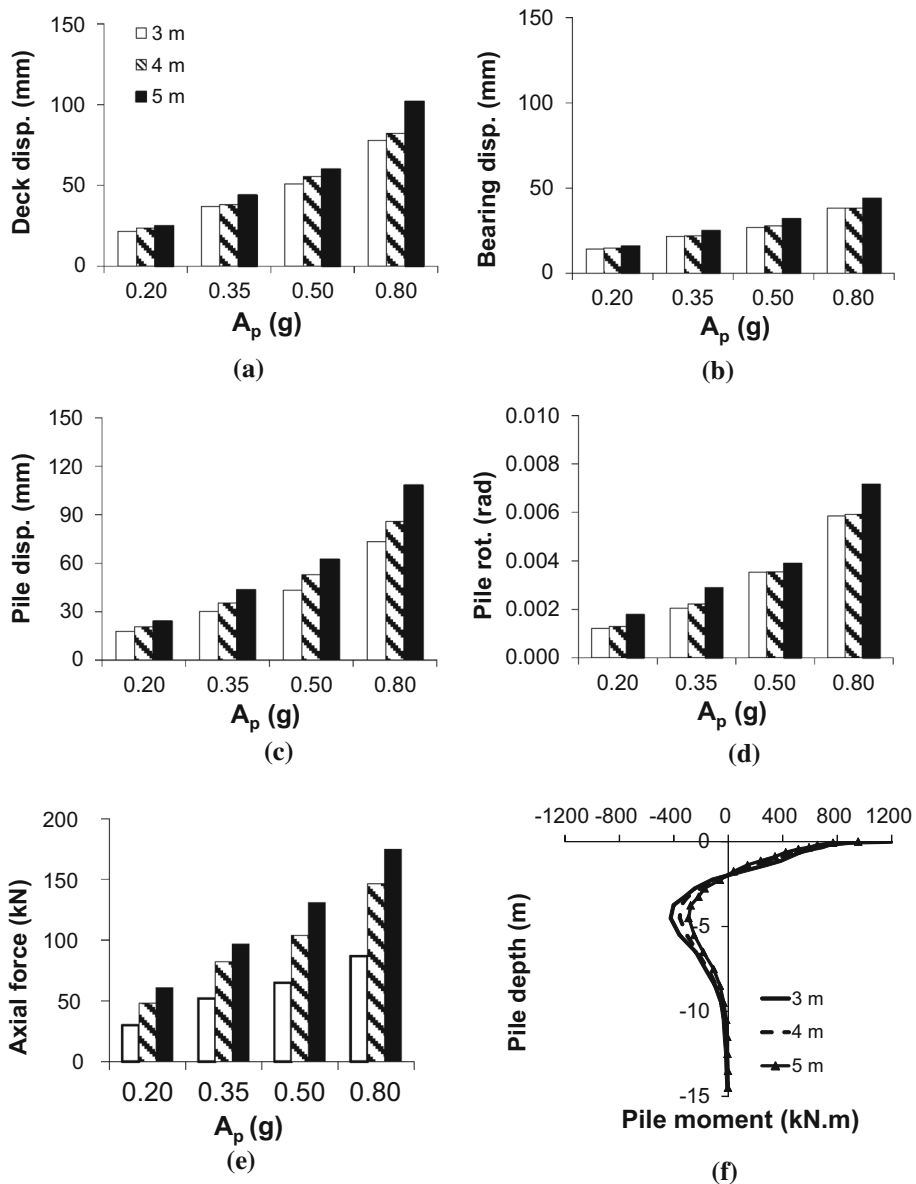


**Fig. 10** **a** Absolute deck displacements, **b** relative bearing displacements, **c** absolute steel H-piles displacements, **d** and rotation, **e** Pile axial forces versus peak ground acceleration for various abutment heights, **f** typical pile moments for San Fernando Earthquake scaled to  $A_p = 0.8$  g

and thicknesses produce larger inertial forces and associated base moments at the bridge (at the bottom of the substructures). These larger base moments need to be counterbalanced by the axial force couples created in the abutment piles at both ends of the bridge. The analysis results also reveal that larger pile moments are observed along the depth of the pile in the case of IBs with shorter and thicker abutments.

### 6.3 Effect of pile size and orientation on deck, bearing, pier and pile responses

The analyses results reveal that the effect of pile size and orientation on the maximum absolute deck and relative bearing displacements as well as pier column drifts and end rotations is not significant. In general, smaller piles oriented to bend about their weak axis produce slightly larger absolute deck displacements especially in the case of large intensity earthquakes.

However, as observed from Fig. 11a–d, the effect of abutment pile size on the absolute pile displacements/end rotations and associated ductilities are found to be significant. The figures reveal that smaller piles are prone to larger absolute displacements especially in the case of large intensity earthquakes due to their smaller stiffness. Similar observations are also made for the absolute pile displacements and end rotations for various pile orientations. That is; larger absolute pile displacements and rotations and associated ductilities are obtained when the piles are oriented to bend about their weak axis. It is noteworthy that larger absolute displacement and rotational ductilities are indicative of larger damage and associated poor seismic performance. Consequently, for IBs having larger piles oriented to bend about their strong axis (stiffer piles), smaller absolute pile displacement and rotational ductilities are expected leading to better seismic performance.

The maximum axial forces and variation of the typical pile moments along the depth of steel H-piles at the abutments are compared for various pile sizes in Fig. 11e, f. Similar results are also obtained for pile orientations. The analyses results reveal that larger or stiffer piles produce larger axial forces in the piles of IBs (but the axial stresses are smaller). It is also observed from Fig. 11f that, the maximum moment occurs at the pile top and larger moments are observed along the depth of the pile in the case of stiffer piles.

### 6.4 Seismic response of the abutment and backfill as a function of the parameters considered

The maximum abutment drifts and moments as well as typical backfill pressure for the longitudinal direction seismic response of the bridge are compared in Fig. 12a–i for various parameters including soil stiffness, abutment height and pile size. The analyses results reveal that stiffer foundation soils combined with taller abutments leads to larger abutment drifts and moments (moment per unit width of abutment: kN.m/m). It is also observed that smaller piles oriented to bend about their weak axis produce larger abutment drifts but smaller abutment moments.

In the case passive backfill pressure however, the pressure behind the abutment is slightly larger in the case of looser foundation soil, taller and thicker abutments as well as smaller piles oriented to bend about their weak axis.

The above observations are mainly due to the fact that the more flexible soil–pile system leads to larger absolute deck displacements as shown in Fig. 9a. Accordingly, the larger absolute displacement of the abutment top towards the backfill in the case of looser foundation soil produces larger backfill deformation and associated larger passive backfill pressures. In the case of taller and thicker abutments, larger absolute deck displacements towards the backfill produce larger backfill deformation and associated passive backfill pressures. In addition, the lower stiffness of smaller piles oriented to bend about their weak



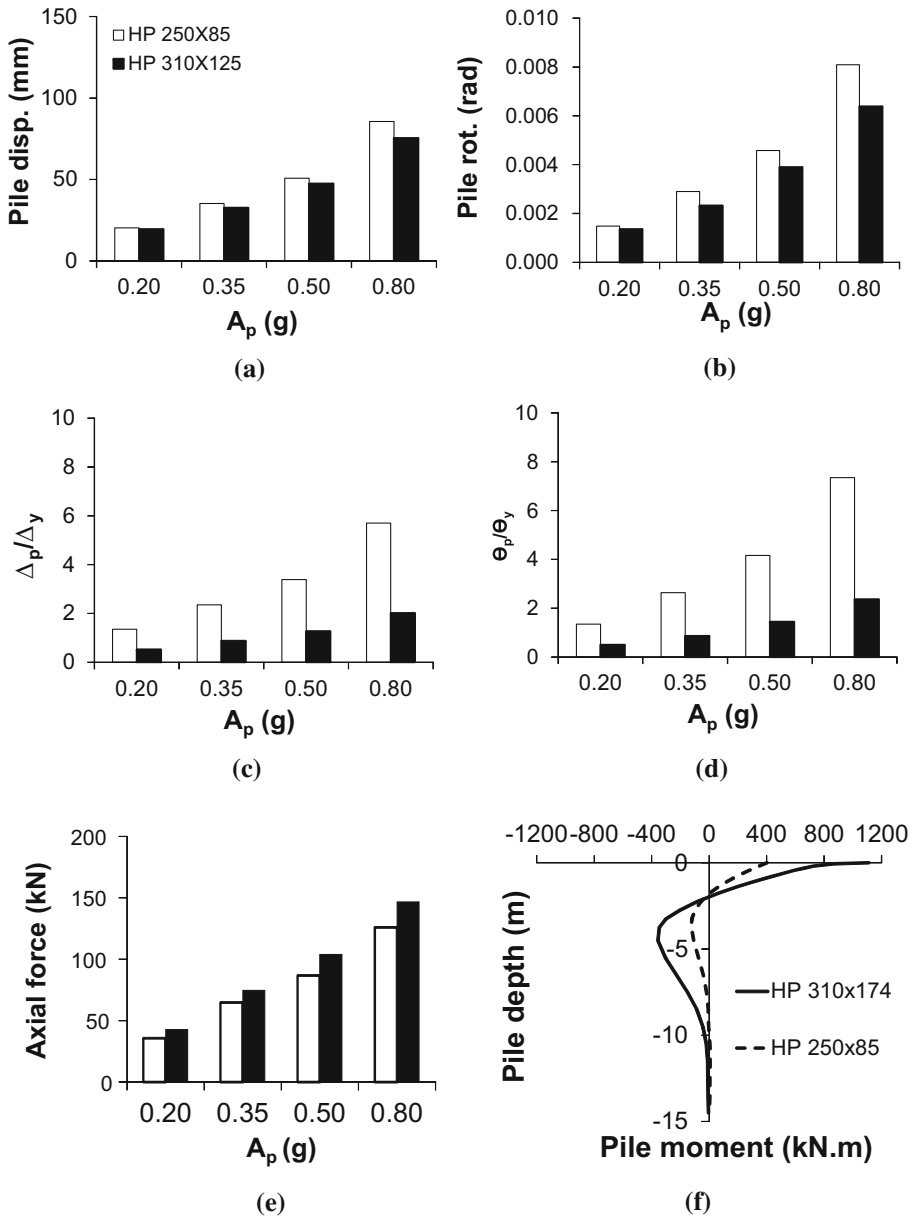


**Fig. 11** **a** Absolute steel H-pile displacements, **b** and rotations, **c** pile displacement ductility and **d** pile rotational ductility, **e** pile axial forces versus peak ground acceleration for various pile sizes. **f** Typical pile moments for San Fernando Earthquake scaled to  $A_p = 0.8$  g

axes provides less resistance against lateral displacements leading to larger relative abutment displacements and provides smaller pile shear forces and moments leading to smaller abutment forces and moments.

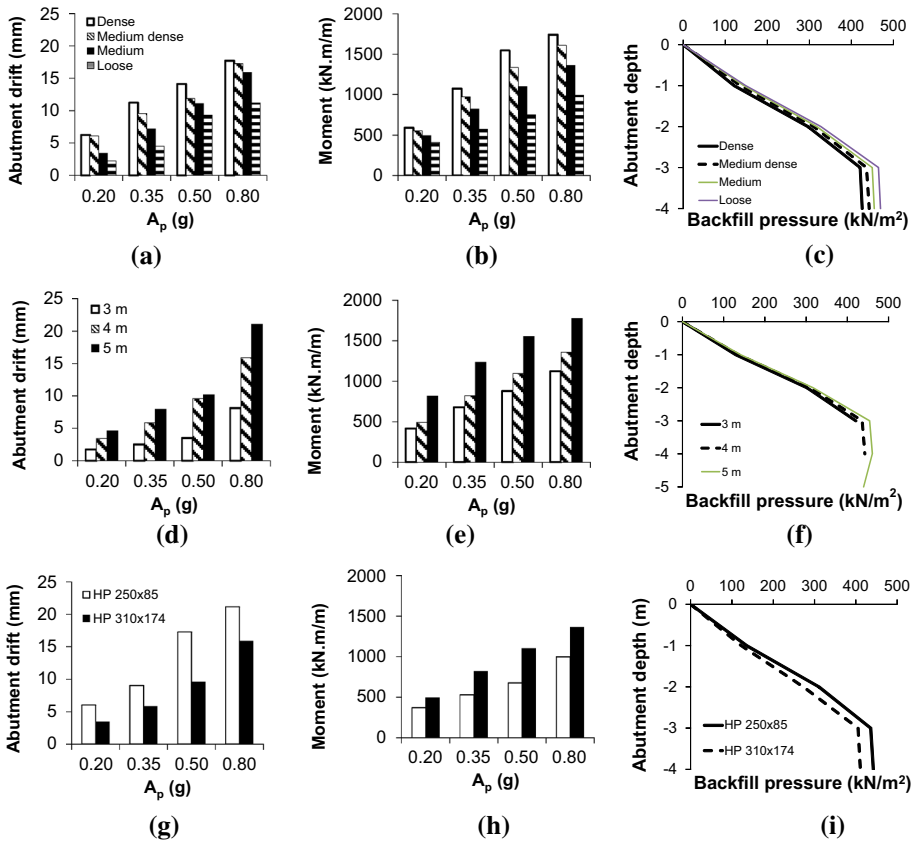


**Fig. 12** **a** Abutment drifts and **b** moments for various foundation soil stiffnesses as a function peak ground acceleration. **c** Typical backfill pressure distribution along the abutment height for various foundation soil stiffnesses and for San Fernando Earthquake scaled to  $A_p = 0.8$  g. **d** Abutment drifts and **e** moments for various abutment heights as a function peak ground acceleration. **f** Typical backfill pressure distribution for various abutment heights and for San Fernando Earthquake scaled to  $A_p = 0.8$  g. **g** Abutment drifts and **h** moments for various pile sizes as a function peak ground acceleration. **i** Typical backfill pressure distribution along the abutment height for various pile sizes and for San Fernando Earthquake scaled to  $A_p = 0.8$  g

## 7 Conclusions

In this paper practical techniques are introduced for detailed modeling of soil–pile and soil–abutment interaction effects for IBs. In addition, sensitivity analyses are conducted to investigate the effect of simplifications and assumptions regarding the embankment model on the seismic response of the benchmark IB considered in the analyses. Furthermore, a parametric study is conducted to determine appropriate structural configurations and geotechnical properties to enhance the seismic performance of IBs.

It is found that while the proposed modeling techniques for IBs are easy to implement in commercially available structural analysis programs, they are also computationally efficient. Using the proposed modeling techniques, the structural model of the benchmark bridge considered in this study is built and sensitivity analyses are conducted to investigate

the effect of various embankment modeling assumptions on the seismic response of the bridge. From the analyses results, the bridge seismic response is found to be insensitive to the length or mass of the embankment and the damping level of the embankment soil used in the model as the free field response is governed by the very large foundation soil unit. However, it is important to note that the modeling techniques used in this study inherently consider uniform deformations along the embankment length, and hence the observations from the sensitivity analyses results may be altered when such deformations are considered. Nonetheless, considering the level of uncertainties in determining the correct soil and backfill properties in the field from practical point of view, the proposed modelling techniques are considered to be adequate for studying the structural response of IBs.

The parametric study revealed that larger flexibility of softer foundation soils provides less fixity to the pier columns and piles, which in turn, reduces the relative displacement and rotation demands on the bridge structural members and generates an IB with a longer fundamental period. The elongation of the fundamental period of the IB-soil system as a unit, evades the high energy content of the earthquake input through the bedrock level producing smaller accelerations and associated inelastic deformations in the structural members of the IB. However, softer foundation soils also produce larger overall absolute deck displacements and slightly larger backfill pressure due to the large lateral deformations of the soil where the IB moves with the foundation soil as a unit.

Furthermore, IBs built with shorter and thinner abutments as well as large steel H-piles oriented to bend about their strong axis are found to exhibit better seismic performance, while the effect of backfill compaction level on the seismic performance of IBs is found to be negligible. The smaller mass of shorter and thinner abutments produces smaller inertial forces acting on the bridge and associated smaller internal forces in IB components leading to better seismic performance. In addition, shorter abutments increase the lateral stiffness of the bridge resulting in smaller seismic displacements. Furthermore, the larger stiffness of larger piles oriented to bend about their strong axis reduces the absolute displacement demands on the deck, the piles themselves and the abutments leading to a better seismic performance.

## References

- AASHTO (2010) Load and resistance factor design (LRFD) specifications. AASHTO, Washington, DC
- Ahn JH, Yoon JH, Kim JH, Kim SH (2011) Evaluation on the behavior of abutment–pile connection in integral abutment bridge. *J Constr Steel Res* 67:1134–1148
- Anandarajah A, Zhang J, Ealy C (2005) Calibration of dynamic analysis methods from field test data. *Soil Dyn Earthq Eng* 25(7–10):763–772
- API (American Petroleum Institute) (2001) Recommended practice and planning, designing, and constructing fixed offshore platforms. API, Washington DC
- Arockiasamy M, Butrieng N, Sivakur M (2004) State-of-the art of integral abutment bridges: design and practice. *J Bridge Eng* 9(5):497–506
- Bhowmick A (2003) Design and construction of integral bridges—an innovative concept. *Indian Concr J* 77(7):1203–1209
- Boulanger RW, Curras CJ, Kutter BL, Wilson DW, Abghari A (1999) Seismic soil–structure interaction experiments and analyses. *J Geotech Geoenviron Eng (ASCE)* 125(9):750–759
- Briseghella B, Zordan T (2015) An innovative steel-concrete joint for integral abutment bridges. *J Traffic Transp Eng* 2(4):209–222
- Cole RT, Rollins KM (2006) Passive earth pressure mobilization during cyclic loading. *J Geotech Geoenviron Eng* 132(9):1154–1164
- Dicleli M (2007) Supplemental elastic stiffness to reduce isolator displacements for seismic-isolated bridges in near fault zones. *Eng Struct* 29(5):763–775

- Dicleli M, Erhan S (2011) Live load distribution formulas for single-span prestressed concrete integral abutment bridge girders. *J Bridge Eng* 14(6):472–486
- Dowell RK, Seible F, Wilson EL (1998) Pivot hysteresis model for reinforced concrete members. *ACI Struct J* 95(5):607–617
- Duncan MJ, Chang CY (1970) Nonlinear analysis of stress and strain in soils. *J Soil Mech Found Div ASCE* 96(5):1629–1653
- Duncan MJ, Mokwa RL (2001) Passive earth pressure: theories and tests. *J Geotechn Geoenviron Eng* 127(3):248–257
- Erhan S (2011) Effect of vehicular and seismic loads on the performance of integral bridges. PhD thesis, Middle East Technical University, Ankara, Turkey
- Faraji S, Ting JM, Crovo DS, Ernst H (2001) Nonlinear analysis of integral bridges: finite element model. *J Geotech Geoenviron Eng* 127(5):454–462
- Fayyadh MM, Akib S, Othman I, AbdulRazak H (2011) Experimental investigation and finite element modelling of the effects of flow velocities on a skewed integral bridge. *Simul Model Pract Theory* 19:1795–1810
- FHWA (1986) Seismic design of highway bridge foundations—volume II: design procedures and guidelines, Publication No. FHWA-RD-94-052. Federal Highway Administration, US Department of Transportation, Washington, DC
- Franchin P, Pinto EP (2014) Performance-based seismic design of integral abutment bridges. *Bull Earthq Eng* 12:939–960
- Itani AM, Sedarat H (2000) Seismic analysis and design of the AISI LRFD design examples of steel highway bridges. Report No. CEER 00-8, Center for Civil Engineering Earthquake Research, University of Nevada, Reno, NV
- Jain SK, Scott RF (1989) Seismic analysis of cantilever retaining walls. In: Proceedings of structural mechanics in reactor technology (SMIRT), Anaheim, California, pp 241–246
- Kalayci E, Civjan SA, Brena SF (2012) Parametric study on the thermal response of curved integral abutment bridges. *Eng Struct* 43:129–138
- Kotsoglou A, Pantazopoulou S (2007) Bridge–embankment interaction under transverse ground excitation. *Earthq Eng Struct Dyn* 36:1719–1740
- Kotsoglou A, Pantazopoulou S (2009) Assessment and modeling of embankment participation in the seismic response of integral abutment bridges. *Bull Earthq Eng* 7:343–361
- Kotsoglou A, Pantazopoulou S (2010) Response simulation and seismic assessment of highway over-crossings. *Earthq Eng Struct Dyn* 39:991–1013
- Maruri R, Petro S (2005) Integral abutments and jointless bridges (IAJB) 2004 survey summary. Federal Highway Administration (FHWA)/Constructed Facilities Center (CFC) at West Virginia University
- Paleo A, Wotherspoon L, Wood J, Chapman H, Scott A, Hogan L, Kivell A, Camnasio E, Yashinsky M, Bruneau M, Chauw N (2011) Lessons learnt from 2011 Christchurch earthquakes: analysis and assessment of bridges. *Bull N Z Soc Earthq Eng* 44(4):319–333
- Petursson H, Kerokoski O (2013) Monitoring and analysis of abutment-soil interaction of two integral bridges. *J Bridge Eng* 18(1):54–64
- ProShake (2009) Version 1.12, EduPro Civil Systems, Inc
- SAP2000 (2010) Integrated finite element analysis and design of structures. Computers and Structures Inc., Berkeley
- Scott A, Civjan SA, Kalayci E, Quinn BH, Brena SF, Allen CA (2013) Observed integral abutment bridge substructure response. *Eng Struct* 56:1177–1191
- Shamsabadi A (2007) Three-dimensional nonlinear seismic soil abutment-foundation-structure interaction analysis of skewed bridges. PhD thesis, University of Southern California, Los Angeles, CA, USA
- Shirato M, Koseki J, Fukui J (2006) A new nonlinear hysteretic rule for winkler type soil–pile interaction spring that consider loading pattern dependency. *Soil Found Jpn Geotechn Soc* 46(2):173–188
- Spyrakos C, Loannidis G (2003) Seismic behaviour of post-tensioned integral bridge including soil–structure interaction. *Soil Dyn Earthq Eng* 23:53–63
- Takeda T, Sozen MA, Nielsen NN (1970) Reinforced concrete response to simulate earthquake. *J Struct Div ASCE* 96(12):2557–2573
- Warn PG, Ryan KL (2012) A review of seismic isolation for buildings: historical development and research needs. *Buildings* 2(3):300–325
- Wotherspoon LM, Bradshaw A, Green RA, Wood C, Palermo A, Cubrinovski M, Bradley BA (2011) Performance of bridges during the 2010 and 2011 Christchurch earthquakes. *Seismol Res Lett* 82(6):950–964
- XTRACT v3.0.7. (2009) Cross-sectional X structural analysis of components. TRC/Imbsen Software Systems, Rancho Cordova

- 
- Zhang J, Makris N (2002) Kinematic response functions and dynamic stiffnesses of bridge embankments. *Earthq Eng Struct Dyn* 31:1933–1966
- Zordan T, Briseghella B, Lanc C (2011) Parametric and pushover analyses on integral abutment bridge. *Eng Struct* 33(2):502–515